ELSEVIER

Biochimica et Biophysica Acta 1192 (1994) 205–214

BBA Biochimica et Biophysica Acta

Bilayer packing characteristics of mixed chain phospholipid derivatives: Raman spectroscopic and differential scanning calorimetric studies of 1-stearoyl-2-capryl-*sn*-glycero-3-phosphocholine (C(18) : C(10)PC) and 1-stearoyl-2-capryl-*sn*-glycero-3-phospho-*N*-trimethylpropanolamine (C(18) : C(10)TMPC)

Michael M. Batenjany [a], Zhao-qing Wang [b], Ching-hsien Huang [b], Ira W. Levin [a,*]

[a] *Laboratory of Chemical Physics, National Institute of Diabetes, and Digestive and Kidney Diseases, National Institutes of Health, Bethesda, MD 20892, USA*

[b] *Department of Biochemistry, Health Sciences Center, University of Virginia, Charlottesville, VA 22908, USA*

(Received 2 November 1993)

Abstract

Raman spectroscopy and high-sensitivity differential scanning calorimetry (DSC) were used to compare the effects of headgroup conformation on the acyl chain packing arrangements in two highly asymmetric phosphatidylcholine (PC) analogues, 1-stearoyl-2-capryl-*sn*-glycero-3-phosphocholine (C(18):C(10)PC) and a polar headgroup derivative of C(18):C(10)PC, 1-stearoyl-2-capryl-*sn*-glycero-3-phospho-*N*-trimethylpropanolamine (C(18):C(10)TMPC), which contains an additional methylene group within the choline moiety; namely, $-P-O-(CH_2)_3-N(CH_3)_3$. The C(18):C(10)TMPC headgroup exhibits an extended *trans* conformation which is independent of bilayer phase. A comparison of gel phase spectral order parameters of the two lipid species indicates a mixed interdigitated state characteristic of three chains per headgroup for C(18):C(10)TMPC. A more intermolecularly ordered liquid crystalline phase is observed, however, for the C(18):C(10)TMPC bilayers. The phase transition cooperative unit size estimated for the C(18):C(10)PC bilayers (~ 140 molecules per unit) is about 7-fold greater than that for the C(18):C(10)TMPC dispersions (~ 20 molecules per unit). We suggest that the extended headgroup for C(18):C(10)TMPC induces a slight tilt in the gel phase packing arrangements for the acyl chains, which may persist in the partially interdigitated liquid crystalline phase bilayer. Macroscopically, tighter packed multilamellar dispersions of C(18):C(10)TMPC occur for systems prepared first in the presence of a higher ionic strength medium. The stacked bilayers may then be transferred to a lower ionic strength environment without loss of their more closely packed adjacent lamellae.

Key words: Raman spectroscopy; DSC; Mixed interdigitated acyl chain bilayer; 1-Stearoyl-2-capryl-*sn*-glycero-3-phosphocholine; 1-Stearoyl-2-capryl-*sn*-glycero-3-phospho-*N*-trimethylpropanolamine; Phosphatidylcholine *trans* headgroup conformation

1. Introduction

The large asymmetry in the hydrocarbon chain lengths of many natural membrane lipids, such as glycosphingolipids, sphingomyelin, cerebrosides and sulfatides, affect significantly both the physical and functional properties of biological membranes [1–4]. For example, lipids with nonuniform acyl chain lengths can provide the bilayer continuity between integral protein surfaces and the bulk lipids of the membrane [5]. Alternatively, bilayer lipids with asymmetric chain structures aggregate to form discrete membrane domains, such as those observed for asymmetric, mixed-chain gangliosides incorporated into 1,2-dimyristoyl-*sn*-glycero-3-phosphocholine (DMPC) liposomes [6]. Morphological changes in phospholipid assemblies also arise when the chain length asymmetry of the lipid molecules increases; that is, the change in geometry

* Corresponding author. Fax: +1 (301) 4960825.

SSDI 0005-2736(94)00060-3

from a cylindrical to an inverted conical configuration has been implicated in initiating the formation of non-lamellar lipid structures [7].

Because the bilayer rearrangements observed in model multilamellar and single shell phospholipid systems dispersed in aqueous media are relevant to the lipid order/disorder characteristics of natural membranes [8], well-defined assemblies of synthetic phosphatidylcholines of these unique asymmetric chain systems present suitable structures for clarifying the critical factors that determine bilayer stability, hydrocarbon chain packing arrangements and thermotropic behavior. For example, vibrational Raman spectroscopic techniques were used to examine the phase transition behavior and chain packing characteristics of aqueous dispersions of a synthetic, asymmetric chain, sphingomyelin (DL-erythro-*N*-lignoceroylsphingosylphosphocholine) for which a low temperature, mixed interdigitated chain gel (II) phase, characterized by a single headgroup area circumscribing three chain cross-sectional areas, converts to a partially interdigitated gel (I) state where the headgroup subtends only two chain areas [9]. At higher temperatures the gel (I) bilayer phase undergoes a second transition to a disordered, partially interdigitated fluid phase. The sensitivity of headgroup substitutions in modulating the packing modifications of interdigitated chain systems was noted in studies involving methyl substitutions at either the 1, 2 or 3 position of the glycerol backbone of the parent dihexadecylphosphatidylcholine (DHPC) system, an ether-linked lipid which, when hydrated, forms a completely interdigitated chain gel phase [10]. For this series of ether lipids the 1-methyl substituted DHPC bilayer, for example, undergoes a dramatic bilayer reorganization which involves the loss of gel phase chain interdigitation [10], again emphasizing the delicate balance of forces that determines a specific hydrocarbon chain arrangement.

In the present study, we utilize Raman spectroscopy and high-sensitivity differential scanning calorimetry (DSC) to contrast the bilayer order/disorder and chain packing parameters of two highly asymmetric phosphatidylcholine (PC) analogues; namely, 1-stearoyl-2-capryl-*sn*-glycero-3-phosphocholine (C(18) : C(10)PC) and a polar headgroup derivative of C(18):C(10)PC, 1-stearoyl-2-capryl-*sn*-glycero-3-phospho-*N*-trimethyl propanolamine (C(18):C(10)TMPC), which contains an additional methylene group in the choline moiety; namely, $-P-O-(CH_2)_3-N(CH_3)_3$. A comparison of the thermodynamic and structural properties of C(18): C(10)TMPC and C(18):C(10)PC bilayers permits one to examine the effects of a subtle headgroup conformational change and headgroup hydration on the acyl chain packing arrangements of assemblies comprised of interdigitated chain phosphatidylcholines. With respect to C(18):C(10)PC, having a conventional phosphatidylcholine *gauche* headgroup geometry, X-ray diffraction studies reveal that fully hydrated dispersions of this asymmetric chain lipid form interdigitated gel phase bilayers in such a manner that the shorter chain of one lipid in a leaflet packs end to end with the analogous chain of a lipid molecule in the opposing leaflet, while the longer *sn*-2 chains position their terminal methyl groups at the water/lipid interface (a mixed interdigitated chain arrangement) [11]. Upon chain melting, the mixed interdigitated chain C(18): C(10)PC bilayers convert directly to a partially interdigitated liquid crystalline phase in which the short *sn*-1 chains of one leaflet pack end to end with the long *sn*-2 chains of the facing monolayer. The vibrational dynamics and packing properties of a series of highly asymmetric chain phosphatidylcholine bilayers were surveyed earlier using, in particular, Raman spectroscopic techniques [12].

Raman spectroscopy offers a sensitive, noninvasive method for assessing the lipid packing characteristics of bilayer aggregates. Specifically, both inter- and intramolecular interactions between acyl chains are monitored by the frequency and intensity changes reflected by the hydrocarbon chain methylene C–H stretching modes in the 2800–3100 cm^{-1} spectral region, while the direct observation of the formation of *gauche* conformers along the acyl chain are reflected by intensity changes in the C–C skeletal stretching modes (1050–1150 cm^{-1} interval). The *gauche* and *trans* conformations of the choline headgroup are delineated directly by the frequency of the C–N stretching modes in the 700–800 cm^{-1} region. Temperature profiles based upon specific Raman spectroscopic peak-height intensity ratios (I_{2850}/I_{2880} and I_{2935}/I_{2880}), derived from the C–H stretching mode interval, are useful in revealing thermodynamic phase transition parameters. For example, for saturated, symmetric chain phosphatidylcholines the amplitude of the gel to liquid crystalline phase transition, determined by the temperature dependence of the methylene C–H stretching mode peak-height intensity parameters, is linearly related to the entropy of the phase transition [13]. A fit of the temperature dependence of these parameters to a two-state thermodynamic model also yields the bilayer transition temperatures, transition widths and Van't Hoff enthalpies [14].

Based on the Raman and DSC data, we distinguish between different acyl chain packing characteristics for the C(18):C(10)PC and C(18):C(10)TMPC bilayers and observe an unusual *trans* headgroup orientation for the C(18):C(10)TMPC dispersions. We estimate from the Raman spectral data a decreased cooperative unit size for the order/disorder phase transition of the C(18):C(10)TMPC bilayers compared to the C(18): C(10)PC system. Finally, the vibrational data also enable us to observe macroscopic changes occurring in

the multilamellar C(18):C(10)TMPC dispersions as a function of ionic strength.

2. Materials and methods

C(18):C(10)PC and C(18):C(10)TMPC were synthesized as previously described [12,15]. Lyophilized powders of these lipids were hydrated in distilled water at a concentration of 20–25% (w/w). Multilamellar dispersions were prepared by cycling the samples 15–18 times through the main lipid transition using a dry ice bath and a water bath, set at 15–20°C above the transition temperature. The multilamellar preparations were then transferred to capillary tubes, spun for 10 min at room temperature using an International Model MB microcapillary centrifuge, flame-sealed and stored at −20°C for 2–5 days prior to the Raman spectral measurements.

An examination of the effects of ionic strength on the interlamellar spacings of the C(18):C(10)PC and C(18):C(10)TMPC preparations involved assemblies reconstituted with 0.15 M $(NH_4)_2SO_4$. The intensity of the ν_1 vibrational mode of the SO_4^{2-} ion at 982.9 cm^{-1} also serves as as internal standard. The preparation of the liposomes was performed as follows. The hydrated multilamellar assemblies were placed in Centricon-3 Concentrators (Amicon, Beverly, MA) and spun at maximum speed for 10 min in an Eppendorf centrifuge (Brinkmann Instruments, Westbury, NY) to remove most of the distilled water. The packed bilayers were resuspended in approximtely 40 volumes of 0.15 M $(NH_4)SO_4$ and respun as above. This process was repeated five times. The bilayers suspended in ammonium sulfate were then cycled 18 times through the main gel to liquid crystalline phase transition using a dry ice bath and a water bath set 15–20°C above the transition temperature. The liposomes were then transferred to capillary tubes, spun for 10 min at room temperature using a microcapillary centrifuge, flame-sealed and stored at −20°C for 2–5 days prior to recording their Raman spectra. The removal of ammonium sulfate was performed in a similar manner, but using distilled water. Samples were cycled and stored as described above. The complete disappearance of the intense 982.9 cm^{-1} feature was taken as an indication of complete removal of ammonium sulfate.

Raman spectra, recorded on a Spex Ramalog 6 dispersive spectrometer equipped with holographic gratings and interfaced to a microcomputer based data acquisition system, were passed to a Sun Unix file server for analysis using locally developed software. An Innova Model 100 argon laser (Coherent Laser Products, Palo Alto, CA) provided 200–250 mW of 514.5 nm laser excitation at the sample. Typically, 5–10 scans were averaged at an instrumental resolution of approx. 5 cm^{-1} and a scan rate of 1 $cm^{-1}\,s^{-1}$. Temperature control was achieved by enclosing the samples in a thermoelectrically regulated cell assembly under computer control. At 200–250 mW, no significant laser heating effects were observed; sample temperatures were accurate to within 0.1°C. Temperature profiles were obtained as previously described [16]. Transition temperatures (T_m) and transition widths (ΔT), as well as Van't Hoff enthalpies were determined from an algorithm based on a two-state thermodynamic model [14]. Cooperative unit sizes were calculated from the ratio of Van't Hoff enthalpy to the calorimetrically determined enthalpy.

High-resolution differential scanning calorimetry was performed on a Microcal MC-2 microcalorimeter equipped with the DA-2 digital interface and data acquisition utility for automatic collection (Microcal, Amhurst, MA). In general, a constant heating scan rate of 15 C°/h was used.

3. Results and discussion

3.1. Gel and liquid crystalline phase raman spectra of C(18):C(10)PC and C(18):C(10)TMPC bilayers

Raman spectra representative of the acyl chain C–H stretching (Figs. 1A and 1B), skeletal C–C stretching (Figs. 1C and 1D) and the choline headgroup C–N stretching mode regions (Figs. 1E and 1F) were recorded for the gel and liquid crystalline phases of hydrated multilamellar dispersions of C(18):C(10)PC and C(18):C(10)TMPC. Since the various band assignments have been discussed previously in detail [16,17], we review here only the salient features.

The symmetric and asymmetric methylene C–H stretching modes, which appear as the intense and partially overlapped features at ~2847 cm^{-1} and ~2882 cm^{-1}, respectively, represent the most prominent gel phase features in the 3100–2800 cm^{-1} spectral region. The broad background beneath the gel phase 2882 cm^{-1} band arises from Fermi resonance interactions between the symmetric methylene stretching fundamental at ~2847 cm^{-1} and the continuum of binary overtones of the 1450 cm^{-1} methylene bending modes representative of the extended all-*trans* hydrocarbon chain [18,19]. A Fermi resonance component of the acyl chain terminal methyl symmetric C–H stretching modes appears at ~2935 cm^{-1}, while the terminal methyl asymmetric C–H stretching modes are present at ~2956 cm^{-1}. Features corresponding to the headgroup choline symmetric and asymmetric methyl C–H stretching modes are observed at ~2960 cm^{-1} and 3042 cm^{-1}, respectively. Above the gel to liquid crystalline phase transition temperature, the gel phase Fermi resonance interactions involving the acyl chain

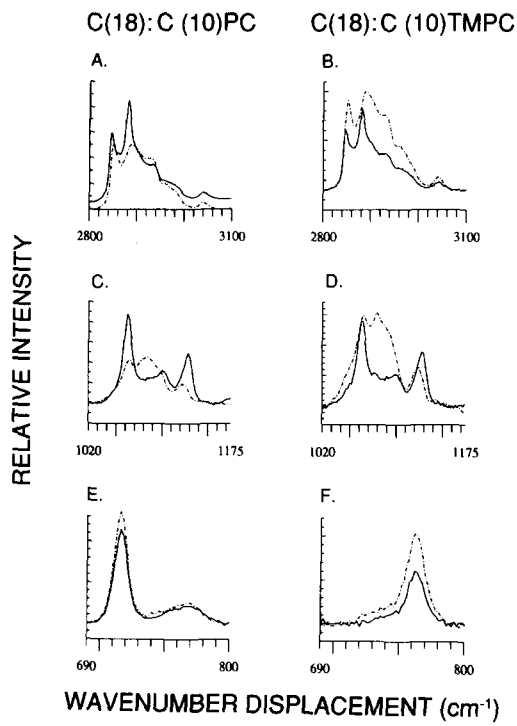

Fig. 1. Typical Raman spectra of gel and liquid crystalline phases for C(18):C(10)PC and C(18):C(10)TMPC multilamellar systems. (A) and (B): Acyl chain methylene C–H stretching modes. (C) and (D): Skeletal methylene C–C stretching modes. (E) and (F): Choline headgroup C–N stretching modes. Solid lines represent gel phases and dot-dashed lines denote liquid crystalline phases. Spectra were collected at a 5 cm^{-1} resolution and baseline corrected.

methylene bending mode overtones diminish because of vibrational decoupling effects along the chain which originate from the introduction of *gauche* conformers along the hydrocarbon chain. For liquid crystalline C(18):C(10)PC bilayers the 2882 cm^{-1} feature shifts upwards by approx. 7 cm^{-1} concomitant with a decrease in the 2900 cm^{-1} background intensity (Fig. 1A). The increased intensity of the 2935 cm^{-1} band, after chain melting, results, in part, from underlying infrared-active, Raman-inactive methylene asymmetric C–H stretching modes that are now Raman allowed because of the disordered chain structures. Thus, the intensities of the 2847 cm^{-1} and the 2935 cm^{-1} bands relative to the intensity of the 2882 cm^{-1} feature reflect directly the state of order or disorder in both the lipid gel and liquid crystalline phases. A comparison of Figs. 1A and 1B, with respect to the relative intensities of the previously noted bands, namely I_{2850}/I_{2880}, indicates that the C(18):C(10)TMPC preparation is more ordered in the liquid crystalline phase than is the C(18):C(10)PC dispersion. Fig. 1B also demonstrates an unusual occurrence for the Raman spectra of lipid systems in that a large increase in integrated intensity occurs for the entire 2800–3100 cm^{-1} region in the liquid crystalline phase compared to the gel phase of this dispersion (see for comparison the conventional example in Fig. 1A). A similar increase in the C(18):C(10)TMPC liquid crystalline phase intensity was observed for the skeletal C–C stretching modes (Fig. 1D), as well as for the choline headgroup C–N stretching mode (Fig. 1F). We interpret these observations as originating in macroscopic changes involving the C(18):C(10)TMPC multilamellar dispersions (vide infra).

The skeletal 1050–1150 cm^{-1} C–C stretching mode regions of both C(18):C(10)PC and C(18):C(10)TMPC bilayers (Figs. 1C and D) directly reflect the intramolecular *trans/gauche* conformational changes within the bilayer acyl chains. The three all-*trans* acyl chain C–C stretching modes are assigned to the bands at 1062 cm^{-1} (out-of-phase skeletal stretching motions), 1100 cm^{-1} and 1129 cm^{-1} (in-phase skeletal stretching motions). Upon chain melting (dot-dash lines, Figs. 1C and 1D), the intensities of the three all-*trans* features decrease and the ~1129 cm^{-1} features shift downward by ~6 cm^{-1}. The 1062 cm^{-1} band shifts to a slightly higher frequency (~1065 cm^{-1}) and a feature at ~1085 cm^{-1}, assigned to *gauche* conformers along the chain, appears [16]. Significantly, the spectra of the gel and liquid crystalline phases of the C(18):C(10)-TMPC bilayers (Fig. 1D) exhibit additional intensity at ~1079 cm^{-1} not seen in the analogous spectra of the C(18):C(10)PC preparation. We assign the 1079 cm^{-1} feature to the PO_2^- symmetric stretching mode in the C(18):C(10)TMPC bilayer. Although this mode is not usually observed in hydrated phosphatidylcholine dispersions, the PO_2^- symmetric stretching mode has been assigned at 1080 cm^{-1} in gel phase 1,2-dipalmitoyl-*sn*-glycero-3-phosphocholine (DPPC) [20] and to a feature at 1082 cm^{-1} in polycrystalline DPPC observed at liquid nitrogen temperatures (unpublished data). Since the observation of the phosphate symmetric stretching modes in the modified trimethylene phosphatidylcholine (TMPC) headgroup analogue is suggestive of a conformational rearrangement within the phosphatidylcholine moiety, we examine the 1020–1150 cm^{-1} region for C(18):C(10)PC and C(18):C(10)TMPC bilayers more closely in Fig. 2. Order/disorder parameters derived from the 1020–1150 cm^{-1} C–C stretching mode region (vide infra) yield T_m values for C(18):C(10)PC and C(18):C(10)TMPC of 15.8 ± 0.2°C and 16.0 ± 0.5°C, respectively (Table 1). Fig. 2A compares spectra at 17°C, within the phase transition region for C(18):C(10)TMPC but after the melting of C(18):C(10)PC, and at 25°C, well into the liquid crystalline phases for both lipid species. At 17°C, C(18):C(10)PC bilayers display a typical liquid crystalline phase, with a prominent band at 1085 cm^{-1}, explicitly due to the presence of the various *gauche* related chain conformers. In contrast, C(18):C(10)-TMPC bilayers, which are in the middle of the phase transition feature, exhibit a peak at ~1078 cm^{-1} (the

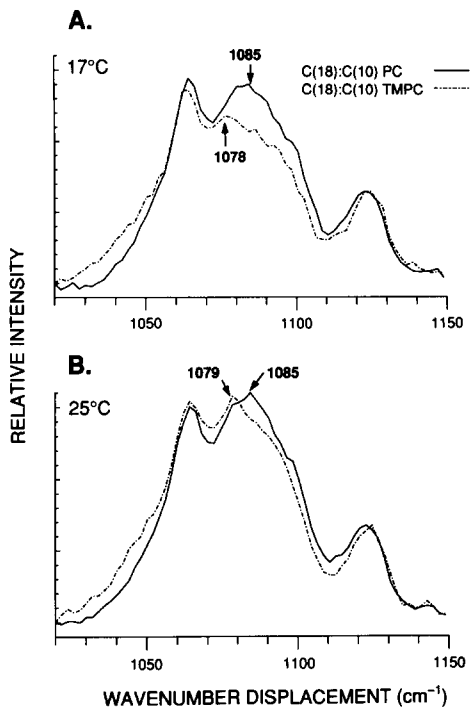

Fig. 2. Typical Raman spectra of skeletal methylene C–C stretching modes for C(18):C(10)PC and C(18):C(10)TMPC multilamellar systems at (A) 17°C and (B) 25°C. Spectra were collected at a 5 cm^{-1} resolution and baseline corrected and normalized to the 1130 cm^{-1} band of the C(18):C(10)TMPC preparation. No smoothing routines were employed.

symmetric PO_2^- stretching mode). After completion of the main phase transition, the C(18):C(10)TMPC spectrum still reflects the phosphate mode at 1079 cm^{-1}, but the region of the spectrum at 1085 cm^{-1} is diminished in intensity relative to the C(18):C(10)PC species. These data indicate that for C(18):C(10)TMPC bilayers in the liquid crystalline phase the PO_2^- symmetric stretching mode is clearly observed and that the intramolecular chain disorder is greater in the liquid crystalline phase of the C(18):C(10)PC dispersions.

We derive information explicitly regarding headgroup orientation in these mixed interdigitated chain phosphatidylcholine analogues by monitoring the 700–800 cm^{-1} C–N symmetric stretching mode region, a spectral interval sensitive to headgroup conformational rearrangements. C(18):C(10)PC displays an intense band at 717 cm^{-1} (Fig. 1E), representative of phosphatidylcholine-containing bilayers reflecting a *gauche* conformation of the $-O-CH_2-CH_2-N^+(CH_3)_3$ segment [21]. In contrast, the comparable C–N symmetric stretching mode for C(18):C(10)TMPC bilayers appears in both the gel and liquid crystalline phases as an intense band at 770 cm^{-1} (Fig. 1F), characteristic of an extended *trans* orientation for the choline moiety [21].

3.2. Acyl chain packing characteristics of C(18):C(10)PC and C(18):C(10)TMPC bilayers: Raman order parameters and calorimetric data

A more detailed understanding of the acyl chain packing characteristics and phase transition cooperativities in the mixed interdigitated chain phosphatidylcholines can be achieved through an examination of the temperature dependence of the various Raman spectroscopic order parameters. The sensitivity to membrane reorganizations of the acyl chain C–H stretching modes around 2847 cm^{-1}, 2882 cm^{-1} and 2935 cm^{-1}, presented as peak-height intensity ratios, provide semi-quantitative measures of bilayer order/disorder properties in both the gel and liquid crystalline phases. In particular, the I_{2850}/I_{2880} parameter directly monitors acyl chain disorder/order arising from lateral chain-chain interactions [22], while the I_{2935}/I_{2880} ratio also furnishes an index of the degree of interchain disorder/order but with superimposed *gauche/trans* isomerization effects [16]. Additionally, in the acyl chain C–C stretching mode region the specific appearance of the *gauche* conformer 1088 cm^{-1} band permits, for example, the I_{1088}/I_{1130} peak-height ratio to be used as a direct probe of the extent of *gauche/trans* isomerization, or intrachain disorder, along the lipid chains. Temperature profiles constructed for the C(18):C(10)PC and C(18):C(10)TMPC preparations using the spectral peak-height ratios I_{1088}/I_{1130}, I_{2850}/I_{2880} and I_{2935}/I_{2880} are shown in Fig. 3. Table 1 summarizes the ascending and descending gel to liquid crystalline phase transition temperature data derived from the Raman spectroscopic and differential scanning calorimetric profiles. A comparison of Figs. 3C and 3D demonstrates an interdigitated gel phase for the C(18):C(10)TMPC dispersion based both

Table 1
Summary of phase transition temperatures (T_m) and transition widths (ΔT) determined from Raman spectroscopic and calorimetric data

	C(18):C(10)PC				C(18):C(10)TMPC			
	heating		cooling		heating		cooling	
	T_m (°C)	ΔT (C°)	T_m (°C)	ΔT (C°)	T_m (°C)	ΔT (C°)	T_m (°C)	ΔT (C°)
I_{2850}/I_{2880}	17.5 ± 0.2	0.6 ± 0.1	17.5 ± 0.2	1.9 ± 0.1	18.2 ± 0.2	3.4 ± 0.1	17.3 ± 0.5	7.0 ± 0.2
I_{2935}/I_{2880}	17.2 ± 0.4	0.5 ± 0.1	17.2 ± 0.4	0.2 ± 0.1	18.3 ± 0.1	3.5 ± 0.1	16.9 ± 0.2	6.5 ± 0.2
I_{1085}/I_{1130}	15.8 ± 0.2	1.5 ± 0.1	15.8 ± 0.2	2.6 ± 0.1	16.0 ± 0.5	5.6 ± 0.1	15.6 ± 0.4	7.7 ± 0.2
DSC	18.8		15.2/17.7		18.1		15.2	

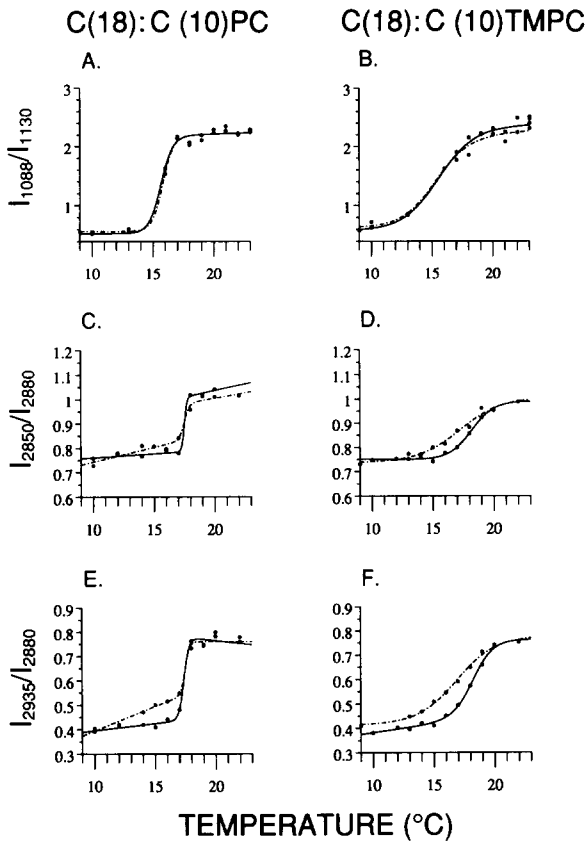

Fig. 3. Temperature profiles for C(18):C(10)PC and C(18):C(10)-TMPC multilamellar dispersions using Raman order parameters derived from the C–C stretching mode I_{1088}/I_{1130} intensity ratios, A and B; the C–H stretching mode I_{2850}/I_{2880} intensity ratios, C and D; and the C–H stretching mode I_{2935}/I_{2880} intensity ratios, E and F. Heating profiles (———), cooling profiles (·–·–·). No computer smoothing routines were applied to the spectra prior to data reduction.

on the similarity of its 10°C gel phase order parameters to those of C(18):C(10)PC bilayers, which are known to adopt a mixed interdigitated gel phase [11] and the diagnostic value for the I_{2850}/I_{2880} peak height intensity parameter [23]. Thus, the I_{2850}/I_{2880} parameter for both dispersions is approx. 0.73, where a noninterdigitated bilayer value is significantly greater at 0.78 [24]. The I_{2935}/I_{2880} values for C(18):C(10)PC and C(18):C10)TMPC are 0.39 and 0.38, respectively. The intrachain order for the two types of assemblies is also the same with I_{1088}/I_{1130} values of about 0.53, reflecting the nearly equivalent intrachain gel phase disorder implied by the I_{2935}/I_{2880} peak intensity ratios. We note, however, considerable differences in the phase transition region for these two types of lipid assemblies. Figs. 3A and 3B, using the intrachain order/disorder I_{1088}/I_{1130} intensity marker, demonstrate an increased breadth, for these sample conditions, of the gel to liquid phase transition of the C(18):C(10)TMPC bilayers (~ 3.7-fold) compared to the C(18):C(10)PC system, which implies a smaller cooperative unit size for the melting process of the species with the *trans* phosphatidylcholine headgroup. Temperature profiles using both the I_{2850}/I_{2880} and the I_{2935}/I_{2880} order parameters to reflect chain-chain interactions also show a decreased phase transition cooperativity for the C(18):C(10)TMPC dispersion. Thus, a comparison of Figs. 3C through 3F demonstrate a broader (6–7-fold) gel to liquid crystalline phase transition width for the C(18):C(10)TMPC dispersion ($\Delta T = 3.5$°C) compared to that of the C(18):C(10)PC preparation ($\Delta T = 0.5$°C). In addition, the smaller liquid crystalline phase order/disorder parameters I_{2850}/I_{2880} for the C(18):C(10) TMPC dispersions (compare Figs. 3C and D) indicate that this system is more ordered in its liquid crystalline phase than that of the C(18):C(10)PC preparations, as noted above. The values for the critical I_{2850}/I_{2880} intermolecular order/disorder parameters are 1.06 and 0.99, determined from ascending temperture profiles, for C(18):C(10)PC and C(18):C(10)TMPC, respectively, where the precision in the peak intensity ratio parameters is ±0.02. This ordering is consistent with the observed decrease in the intensities of the 2847 cm^{-1} and the 2935 cm^{-1} bands relative to the intensity of the 2882 cm^{-1} feature seen in the C(18):C(10) TMPC liquid crystalline phase compared to that of the C(18):C(10)PC system (see Figs. 1A and 1B). Fig. 3 shows that the temperature profiles based on the C–H stretching mode region intensity parameters exhibit greater hysteresis behavior for the C(18):C(10)TMPC bilayers, whose polar headgroups are extended, in contrast to those determined for the C(18):(C10)PC dispersions. The Raman spectroscopic data for the descending temperature profiles in Fig. 3 indicate that significant hysteresis effects arise in only the interchain I_{2850}/I_{2880} and I_{2935}/I_{2880} parameters but not the intrachain I_{1085}/I_{1130} index. If the gel phase chains of the C(18):C(10)TMPC species are tilted because of the extended, *trans* headgroup conformation (in contrast to the straight chains in C(18):C(10)PC), a hysteresis effect for the values of T_m in the descending temperature profile might be expected as the chains 'anneal' to the more stable, interdigitated form; that is, a kinetic effect dominates as the gel state is approached from the liquid crystalline phase. As shown in Table 1 for the ascending temperature profiles, the T_m values reflecting *gauche/trans* isomerization, derived from the I_{1085}/I_{1130} ratios, for both lipid species occur prior to the T_m values related to chain spreading, reflected by the I_{2850}/I_{2880} and I_{2935}/I_{2880} indices. That is, the mixed interdigitated, three chain per headgroup packing arrangement probably prevents a disordering of the lattice in terms of decreased chain-chain interactions until the lattice accommodates to the increased acyl chain *gauche* conformers formed on increasing temperature.

In agreement with the Raman temperature profiles, the DSC data for the C(18):C(10)PC preparation exhibits a sharp transition in its heating cycle (Fig. 4A), while the C(18):C(10)TMPC preparation (Fig. 4C) displays a broader main transition (> 3-fold). The increased breadth of the gel to fluid phase transition in the C(18):C(10)TMPC system again implies a decreased cooperative unit size for the melting of these bilayers compared to those of C(18):C(10)PC. The Van't Hoff enthalpies (Table 2) of these two PC analogs, estimated from fitting the Raman spectral I_{2935}/I_{2880} temperature profiles (Figs. 3E and 3F) to the two-state thermodynamic model [14], and the calorimetric enthalpies were used to calculate cooperative unit sizes. The C(18):C(10)PC bilayers show a cooperative unit size of ~ 140 molecules, while the C(18):C(10)TMPC bilayers demonstrate a significantly smaller cooperative unit size of ~ 20 molecules. Both are much lower than cooperative unit size estimates of typical saturated, symmetric chain PCs obtained from Raman spectroscopic data in our laboratory. For example, using the analogous approaches and similarly purified lipids, we find that for typical DMPC bilayers, upon fitting the I_{2935}/I_{2880} temperature profile to a two-state thermodynamic model as above, a Van't Hoff enthalpy (ΔH_{VH}) of ~ 2044 kcal mol^{-1}, which when divided by the calorimetric ΔH of ~ 5.4 kcal mol^{-1} [25], results in a cooperative unit size estimate of ~ 450 molecules.

The cooling scan of the C(18):C(10)PC dispersion (Fig. 4B) exhibits two distinct peaks at 17.7°C and 15.2°C, while that of the C(18):C(10)TMPC preparation (Fig. 4D) displays a single transition at 15.2°C. The cooling profile derived for C(18):C(10)PC from the I_{2935}/I_{2880} spectral indices in Fig. 3E is consistent with the descending calorimetric trace of Fig. 4B. That is, a sharp transition, of about three-quarters the amplitude of the gel to liquid crystalline phase transition, is observed on cooling. For this descending temperature profile, the Raman spectral order parameters of the gel phase then decrease linearly as the temperature of the sample decreases from 17°C to 10°C. In the ascending temperature profile the gel phase shows essentially no increase in the order/disorder parameters across the 8–16°C temperature interval. Thus, in the Raman descending temperature profile, the lower transition sensed by the calorimeter in Fig. 4B may, in actuality, be represented by the change in the order/disorder parameters observed around 15°C. The presence of two distinct peaks in the descending calorimetric scan of the C(18):C(10)PC dispersion is perhaps analogous to the Raman spectral studies referred to above on the highly asymmetric synthetic sphingomyelin system [9]. That is, on cooling, C(18):C(10)PC passes first through a metastable partially interdigitated gel phase before achieving the stable mixed interdigitated gel state. In contrast, the liquid crystalline phase of C(18):C(10)-TMPC, which is more ordered than that of the C(18):C(10)PC analogue, appears to form the mixed interdigitated chain arrangement directly, as implied by the lack of multiple peaks in the DSC cooling curve (Fig. 4D).

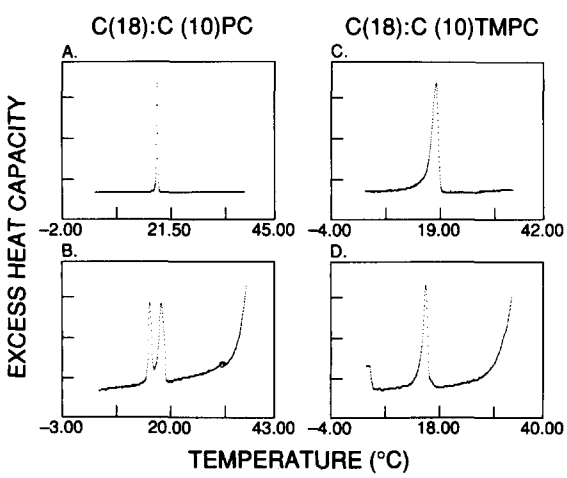

Fig. 4. Temperature profiles for C(18):C(10)PC and C(18):C(10) TMPC multilamellar dispersions from differential scanning calorimetry. (A and C) Heating profiles; (B and D) Cooling profiles.

Table 2
Summary of phase transition calorimetric (ΔH_{cal}) and Van't Hoff (ΔH_{VH}) enthalpies, entropies (ΔS) and cooperativities for C(18):C(10)PC and C(18):C(10)TMPC bilayers

	C(18):C(10)PC	C(18):C(10)TMPC
ΔH_{cal} (kcal mol^{-1})	9.0	9.3
ΔS (cal/mol)	31.2	30.8
ΔH_{VH} (kcal mol^{-1}) [a]	1280.15	198.3
Cooperative unit size (molecules)	~ 142	~ 21

[a] Determined from the Raman spectroscopic I_{2935}/I_{2880} temperature profiles.

We suggest a general model for the packing of the acyl chains of the hydrated C(18):C(10)TMPC assembly. Hauser et al. [26] have compared phosphatidylethanolamine, with its smaller headgroup size, and phosphatidylcholine structures in both polycrystalline and fully hydrated multilamellar systems. They conclude that the larger phosphatidylcholine headgroup could result in one of three conformations for a lipid system: (1) a tilted headgroup; (2) a sawtooth arrangement for the polar headgroups; or (3) an acyl chain tilt to satisfy the headgroup to acyl chain cross-sectional mismatch. With respect to mixed interdigitated chain systems, X-ray studies have already demonstrated a straight chain orientation for C(18):C(10)PC bilayers [11]. For the larger, extended C(18):C(10)TMPC headgroup, it appears reasonable to suggest that the acyl chains would adopt a slightly tilted orientation, which

would be consistent with the similarity to C(18):C(10)-PC in its ΔH and ΔS values determined calorimetrically (see, Table 2), as well as the smaller cooperative unit size for the C(18):C(10)TMPC phase transition. Additionally, the cooling temperature profiles obtained both calorimetrically and from the I_{2935}/I_{2850} Raman spectroscopic parameters, which reflect primarily chain characteristics, display different behavior for the C(18)C:(10)PC and C(18):C(10)TMPC species, which again reinforces the notion that the acyl chains of the system with the increased headgroup size pack other than in a straight chain arrangement. In general, chain tilt is induced when the headgroup area is greater than that of the chain area in order to maintain the requisite close packing characteristics of the chains in the gel bilayer matrix.

3.3. Macroscopic changes in the C(18):C(10)TMPC multilamellar system

In addition to leading to a putative tilted chain packing arrangement for the gel phase bilayer, the extended, *trans* headgroup conformation for C(18):C(10)TMPC may induce increased intermolecular interactions between headgroups of adjacent bilayers within a multilamellar assembly. Fig. 5 compares the spectral contours in the 2900 cm^{-1} C–H stretching mode region of the gel and liquid crystalline phases of C(18):C(10)PC and C(18):C(10)TMPC when dispersed first in water (Figs. 5A and 5B) then 0.15 M $(NH_4)_2SO_4$ (Figs. 5C and 5D). The ammonium sulfate is washed out to return the solution to low ionic strength conditions (Figs. 5E and 5F). The spectra of the C(18):C(10)PC preparation in Figs. 5A and 5C are similar to those of the C(18):C(10)TMPC dispersions in Figs. 5D and 5F in which a diminished liquid crystalline phase intensity occurs relative to the gel phase intensity. However, when first preparing C(18):C(10)-TMPC in water, the liquid crystalline phase intensity across the 2800–3100 cm^{-1} interval (Fig. 5B) appears, in contrast, to C(18):C(10)PC (Fig. 5A) to be greater. Integrated intensity values across the 2900 cm^{-1} spectral region for the gel (G)/liquid crystalline (L) phases, which are proportional to the number of molecular scatterers excited by the the laser radiation, give G/L ratios for the initial water dispersions (Figs. 5A and 5B) of 1.06 and 0.59 for C(18):C(10)PC and C(18):C(10)TMPC bilayers, respectively. However, after the ammonium sulfate exposure and subsequent removal (Figs. 5E and 5F), we observe G/L ratios of 1.07 and 0.98 for C(18):C(10)PC and C(18):C(10)TMPC bilayers, respectively, indicating that the integrated intensity parameters are only changing for the C(18):C(10)-TMPC dispersions prepared at low ionic strength.

By normalizing the integrated intensities of the C–H stretching mode regions of the C(18):C(10)PC and C(18):C(10)TMPC dispersions to an internal standard, namely, the integrated intensity of the ν_1 mode of SO_4^{2-} at 982.9 cm^{-1} (data not shown) [16], we conclude that the liquid crystalline phases of the C(18):C(10)PC and C(18):C(10)TMPC bilayers exhibit almost identical intensity values. However, the integrated intensity for the C(18):C(10)TMPC gel phase is about half that of the C(18):C(10)PC dispersion. To exclude the possibility that the C(18):C(10)TMPC intrabilayer acyl chain packing arrangements differ between the low and high ionic strength conditions, we compared the lateral, chain-chain I_{2850}/I_{2882} indices. At gel phase temperatures of 10 and 9°C, respectively, the C(18):C(10)TMPC dispersions give similar values of 0.72 (low ionic strength, Fig. 5B) and 0.73 (after treatment under high ionic strength conditions, Fig. 5D). (The 9°C order parameter was extracted from the descending temperaure profile; the precision of the order parameters is ±0.02.) Additionally, the I_{2935}/I_{2880} order parameters for C(18):C(10)TMPC for the two different treatments regarding ionic strengh are 0.38 and 0.39, respectively. The similarities in the vari-

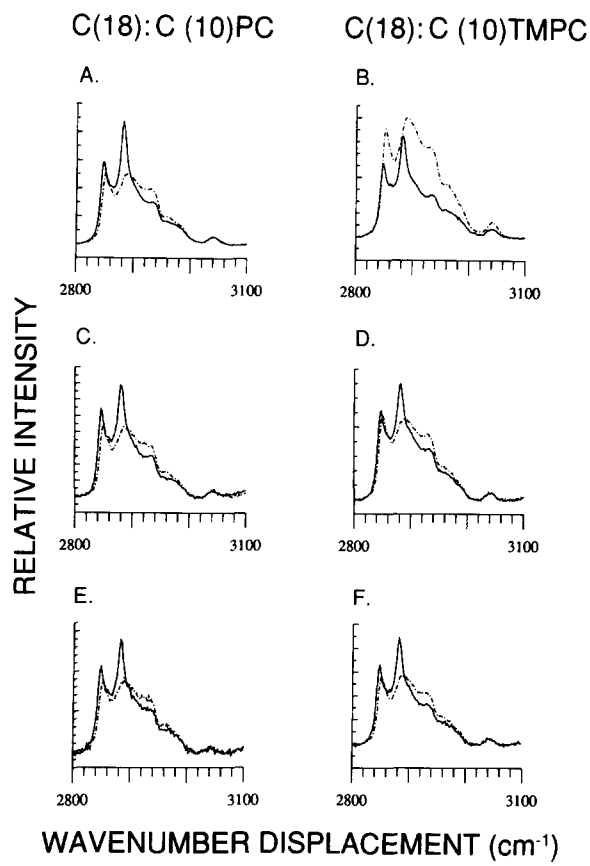

Fig. 5. Relative intensity profiles of acyl chain methylene C–H stretching modes for C(18):C(10)PC and C(18):C(10)TMPC multilamellar dispersions. (A and B) low ionic strength (distilled water); (C and D) high ionic strength (0.15 M ammonium sulfate); (E and F) return to low ionic strength (distilled water). No computer smoothing routines were applied to the spectra. See text for details.

ous order parameters suggest that the unusual, observed increase in integrated intensity of the 2800–3100 cm^{-1} region upon chain melting of C(18):C(10)TMPC bilayers is macroscopic in nature and does not involve a rearrangement within the bilayer matrix itself. Thus, the spectral data associated particularly with Fig. 5B suggest that while the C(18):C(10)TMPC liquid crystalline phase intensity behaves normally relative to other phosphatidylcholine dispersions, the decreased C(18):C(10)TMPC gel phase intensity implies an increased gel phase interbilayer distance. Since the liquid crystalline intensity of C(18):C(10)TMPC behaves in a conventional manner, we speculate that upon melting, the C(18):C(10)TMPC interbilayer distances decrease.

Interbilayer repulsion effects can account for the spectral intensity changes in the C(18):C(10)TMPC dispersions as a function of ionic strength. That is, for the gel phase the extended *trans* conformation of the C(18):C(10)TMPC headgroup separates the $(CH_3)_3N$– group from the phosphate oxygens; hence, diminishing the shielding effects of the choline methyl groups. The isolated, negatively charged phosphate moieties would exhibit an increased hydration repulsion effect between opposing bilayers of the multilamellar assembly. However, on heating, the large network of surface-structured water reorganizes, increasing the overall entropy of the system and resulting in a more closely packed multilamellar liquid crystalline phase whose integrated spectral intensity across the 2800–2900 cm^{-1} reflects the usual values. Thus, increasing the initial ionic strength of the C(18):C(10)TMPC dispersion with 0.15 M $(NH_4)_2SO_4$ probably diminishes the hydration repulsion between opposing bilayers by displacing some of the hydration shells about the $(CH_3)_3N$– group and the phosphate oxygens; an effect which would now allow a closer, more effective stacking of the adjacent bilayers. Once formed, the multilamellar assembly appears to be relatively stable, as observed upon the removal of ammonium sulfate (Fig. 5F). (Removal of ammonium sulfate is monitored by the disappearance of the intense 982.9 cm^{-1} feature characteristic of the SO_4^{2-} ion.) A similar phenomenon has been observed, for example, in the Mn^{2+}-DNA system [29], where heating the system results in bringing the DNA strands closer together. The driving force for bringing the DNA molecules closer was suggested to arise from the entropic gain obtained when surface-structured water about the isolated phosphate moieties is released [29].

4. Summary

The use of vibrational Raman spectroscopy and high sensitivity differential scanning calorimetry provides a detailed comparison of two related synthetic, mixed interdigitated chain bilayer assemblies, C(18):C(10)PC and C(18):C(10)TMPC, where the latter lipid species possesses an additional methylene group within the polar phosphatidylcholine headgroup moiety. The data demonstrate that the C(18):C(10)PC bilayers exhibit larger phase transition cooperative unit sizes in comparison to the properties of the C(18):C(10)TMPC dispersions. In contrast to the C(18):C(10)PC *gauche* headgroup conformation, the C(18):C(10)TMPC system exhibits an extended *trans* conformation of the choline moiety in both the gel and liquid crystalline phases, which may partially shield the *sn*-1 chain terminal methyl groups from exposure to water in the fully interdigitated gel phase. The extended C(18):C(10)-TMPC *trans* headgroup conformation alters the electrostatic considerations between the charged centers of the headgroup. This leads to an increase in the polarizability changes for the phosphate symmetric stretching mode at 1079 cm^{-1}, which now strongly appears in the liquid crystalline phase above the background of acyl chain *gauche* conformers centered around 1085 cm^{-1}. We suggest that the extended headgroup in the C(18):C(10)TMPC dispersion induces a slight tilt in the gel phase packing arrangements for the acyl chains and an ordering of the liquid crystalline phase bilayer. Finally, it appears that macroscopically, tighter packed multilamellar dispersions of C(18):C(10)TMPC can be achieved if prepared first in the presence of a higher ionic strength medium. The stacked bilayers can then be transferred to a lower ionic strength environment without loss of their more tightly packed adjacent lamellae.

References

[1] O'Brien, J.S. and Rouser, G. (1964) J. Lipid Res. 5, 339–342.
[2] Barenholz, Y. and Thompson, T.E. (1980) Biochim. Biophys. Acta 604, 129–158.
[3] Calhoun, W.I. and Shipley, G.G. (1980) Biochim. Biophys. Acta 555, 436–441.
[4] DeVries, G.H. and Norton, W.T. (1974) J. Neurochem. 22, 251–257.
[5] Gerristen, W.J., Van Zoelen, E.G.G., Verkleij, A.M., De Kruijff, B. and Van Deenen, L.L.M. (1980) Biochim. Biophys. Acta 551, 248–259.
[6] Tillack, T.W., Wong, M., Alietta, M. and Thompson, T.E. (1980) Biochim. Biophys. Acta 691, 1261–273.
[7] Huang, C., and Mason, J.T. (1986) Biochim. Biophys. Acta 864, 423–470.
[8] Nagle, J.F. (1980) Annu. Rev. Phys. Chem. 31, 157–195.
[9] Levin, I.W., Thompson, T.E., Barenholz, Y. and Huang, C. (1985) Biochemistry 24, 6282–6286.
[10] Lewis, E.N., Bittman, R. and Levin, I.W. (1986) Biochim. Biophys. Acta 861, 44–52.
[11] McIntosh, T.J., Simon, S.A., Ellington, J.C. and Porter, N.A. (1984) Biochemistry 23, 4038–4044.
[12] Huang, C., Mason, J.T. and Levin, I.W. (1983) Biochemistry 22, 2775–2780.
[13] Huang, C., Lapides, J.R. and Levin, I.W. (1982) J. Am. Chem. Soc. 104, 5926–5930.

[14] Kirchhoff, W.H., Levin, I.W. (1987) J. Res. Natl. Bur. Stds. 92, 113–128.
[15] Isaacson, Y.A., Deroo, P.W., Rosenthal, A.F., Bittman, R., McIntyre, J.O., Bock, H.-G., Gazzotti, P. and Fleischer, S. (1979) J. Biol. Chem. 254, 117–126.
[16] Levin, I.W. (1984) in Advances in Infrared and Raman Spectroscopy (Clark, R. and Hester, R., eds.), Vol. 11, pp. 1–48, Wiley Heyden, New York.
[17] Bryant, G.J., Lavialle, F. and Levin, I.W. (1982) J. Raman Spectroscopy 12, 118.
[18] Snyder, R.G. Hsu, S.L. and Krimm, S. (1978) Spectrochim. Acta 34A, 395–406.
[19] Snyder, R.G and Scherer, J.R. (1979) J. Chem. Phys. 71, 3221–3228.
[20] Spiker, R.C. and Levin, I.W. (1975) Biochim. Biophys. Acta 388, 361–373.
[21] Akutsu, H. (1981) Biochemistry 20, 7359–7366.
[22] Mushayakarara, E., Albon, N. and Levin, I.W. (1982) Biochim. Biophys. Acta 686, 153–159.
[23] O'Leary, T.J. and Levin, I.W. (1984) Biochim. Biophys. Acta 766, 185–189.
[24] Vincent, J.S., Revak, S.D., Cochrane, C.G. and Levin, I.W. (1991) Biochemistry 30, 8395–8401.
[25] Wilkinson, D.A. and Nagle, J.F. (1981) Biochemistry 20, 187–192.
[26] Hauser, H., Pascher, I., Pearson, R.H. and Sundell, S. (1981) Biochim. Biophys. Acta 650, 21–51.
[27] Pearson, R.H. and Pasher, I. (1979) Nature 281, 499–501.
[28] Büldt, G., Gally, H.U., Seelig, J. and Zaccai, G. (1979) J. Mol. Biol. 134, 673–691.
[29] Rau, D.C. and Parsegian, V.A. (1992) Biophys. J. 61, 260–271.
[30] Pascher, I., Sundell, S. and Hauser, H. (1981) J. Mol. Biol. 153, 791–806.